Thermodynamics of doping and vacancy formation in $BaZrO_3$ perovskite oxide from density functional calculations

Per G. Sundell, Mårten E. Björketun, and Göran Wahnström
Department of Applied Physics, Chalmers University of Technology, S-412 96 Göteborg, Sweden
(Received 19 October 2005; revised manuscript received 12 January 2006; published 20 March 2006)

Density functional calculations combined with thermodynamical modeling have been used to investigate defect formation in a perovskite-structured oxide in equilibrium with an oxygen containing atmosphere. We have calculated the electronic structure and formation energies for anion and cation vacancies and for Ga, Gd, In, Nd, Sc, and Y dopants incorporated on different lattice sites in $BaZrO_3$. On energetic grounds, it is found that most of the investigated dopants (with the possible exception of Nd and Gd) preferably substitute for Zr atoms in the lattice. The interaction between dopants was found to be repulsive and correlated with the ionic radius of the dopant, while the dopant-oxygen vacancy interaction was found attractive. We also show that oxygen vacancies are not thermodynamically stable at low temperatures, but will form at the high temperatures and low oxygen partial pressures typically used during synthesis of the material.

DOI: 10.1103/PhysRevB.73.104112 PACS number(s): 61.72.Ji, 71.55.Ht, 71.15.Mb

I. INTRODUCTION

A range of materials based on perovskite-structured oxide ceramics have oxygen-ion- and proton-conducting properties and might be used in various electrochemical applications such as fuel cells, gas sensors, and hydrogen pumps.[1] These perovskite oxides become proton conductors after doping with lower valence cations followed by exposure to a humid atmosphere. It is believed that the doping results in the formation of a high concentration of charge-compensating oxygen vacancies and that protonic defects can be introduced via dissociative absorption of water from the gas phase into the vacancies.[2,3] Therefore, a detailed understanding of the defect chemistry on a microscopic level is essential in order to optimize the performance of these materials.

Several theoretical studies of defect formation in perovskite oxides have successfully employed model potentials to calculate the formation energies of intrinsic defects, solution energies of impurity atoms, and activation energies for ionic migration.[4–7] However, simulations based on first principles are valuable in order to understand the electronic mechanisms involved in the defect formation process.[8–11] This is particularly important for wide-band-gap semiconductors and insulators, where charge transfer can be expected to take place among the defect levels introduced by dopants, vacancies, and interstitials.[12–14] Since most commonly used approaches—such as density functional theory (DFT)—are to be considered as zero-temperature, zero-pressure techniques, direct comparison with experiments carried out at ambient conditions is not straightforward.[15] Recent studies of defect formation in oxides have therefore combined density functional simulations with thermodynamics in order to take into account the effects of different environmental conditions,[8,16] as well as finite temperature and pressure.[17]

In the present work, we have investigated the defect properties of $BaZrO_3$ doped with various trivalent cations. This material appears to combine a high proton conductivity with good chemical and mechanical stability,[18–20] which makes it a promising candidate for solid-oxide fuel-cell (SOFC) applications. However, the reported values of the bulk conductivity of Y-doped $BaZrO_3$ appear to vary several orders of magnitude at a given temperature,[18,21–23] indicating that the electrical and ionic conducting properties might depend strongly on the sample preparation conditions.[24] To address these issues, we have used DFT-based calculations in conjunction with thermodynamic modeling to investigate vacancy formation and solution of Ga, Gd, In, Nd, Sc, and Y dopants in $BaZrO_3$ in equilibrium with an oxygen-containing atmosphere. Our results give support to the conclusion that the environmental conditions during processing (chemical potentials, oxygen partial pressure, and temperature) may significantly influence the behavior of ionic conducting oxides in actual applications.[3]

II. BASIC FORMALISM

The necessary formalism to determine defect concentrations and defect levels in semiconductors from first-principles total-energy calculations has been well established during the last decade.[25–27] More recently, it has also been demonstrated how such results can be extended to finite temperature and pressure.[15,28] In this section, we will apply the formalism to a $BaZrO_3$ crystal in contact with an oxygen-containing atmosphere.

A. Defect formation energies

Defect formation energies can be defined as the total energy of the system containing a defect minus the total energy of the perfect system. When investigating defects that change the composition of a material, the formation energies are usually evaluated with respect to a set of fixed external chemical potentials for the atomic species involved.[25,26] The results will then depend on the actual values of these atomic chemical potentials and, in the case of charged defects, on the chemical potential of electrons in the material (i.e., the Fermi energy).[29] For instance, the total energy required to create an oxygen vacancy (V_O) in charge state q can be calculated from the difference in total energy E^{tot} of two supercells containing n primitive cells as[8]

$$\Delta E^{f}_{V_{\mathrm{O}},q} = E^{\mathrm{tot}}[n(\mathrm{BaZrO}_{3-1/n});q] - E^{\mathrm{tot}}[n(\mathrm{BaZrO}_3)] + \mu_{\mathrm{O}} + q\mu_{\mathrm{e}}, \quad (1)$$

where $1/n$ is the effective vacancy concentration, μ_{O} is the chemical potential of oxygen atoms, and μ_{e} is the chemical potential of electrons. By $E^{\mathrm{tot}}[\ldots;q]$ we denote the total energy of a supercell where the number of electrons has been adjusted to create a defect in charge state q. In the same way the formation energies of a barium vacancy (V_{Ba}) or a zirconium vacancy (V_{Zr}) can be calculated as

$$\Delta E^{f}_{V_{\mathrm{Ba}},q} = E^{\mathrm{tot}}[n(\mathrm{Ba}_{1-1/n}\mathrm{ZrO}_3);q] - E^{\mathrm{tot}}[n(\mathrm{BaZrO}_3)] + \mu_{\mathrm{Ba}} + q\mu_{\mathrm{e}}, \quad (2)$$

$$\Delta E^{f}_{V_{\mathrm{Zr}},q} = E^{\mathrm{tot}}[n(\mathrm{BaZr}_{1-1/n}\mathrm{O}_3);q] - E^{\mathrm{tot}}[n(\mathrm{BaZrO}_3)] + \mu_{\mathrm{Zr}} + q\mu_{\mathrm{e}}, \quad (3)$$

where μ_{Ba} and μ_{Zr} are the chemical potentials of Ba and Zr atoms, respectively. Finally, the solution energy of a dopant atom M on a barium site (M_{Ba}) or a zirconium site (M_{Zr}) can be calculated as the total energy difference[16]

$$\Delta E^{f}_{M_{\mathrm{Ba}},q} = E^{\mathrm{tot}}[n(\mathrm{Ba}_{1-1/n}M_{1/n}\mathrm{ZrO}_3);q] - E^{\mathrm{tot}}[n(\mathrm{BaZrO}_3)] + \mu_{\mathrm{Ba}} - \mu_M + q\mu_{\mathrm{e}} \quad (4)$$

$$\Delta E^{f}_{M_{\mathrm{Zr}},q} = E^{\mathrm{tot}}[n(\mathrm{Ba}M_{1/n}\mathrm{Zr}_{1-1/n}\mathrm{O}_3);q] - E^{\mathrm{tot}}[n(\mathrm{BaZrO}_3)] + \mu_{\mathrm{Zr}} - \mu_M + q\mu_{\mathrm{e}}, \quad (5)$$

where $1/n$ is the effective dopant concentration and μ_M denotes the chemical potential of the dopant.

When considering defect formation in the dilute limit, care must be taken to choose a sufficiently large supercell to avoid any spurious interactions between defects in neighboring cells.[10] This is particularly important for charged defects, which may induce long-range lattice relaxations in a material.[29] However, defect interactions are interesting in their own right, since they may result in important phenomena such as dopant clustering, or "trapping," of oxygen vacancies near dopants. The interaction energy ΔE^{int} for a pair of point defects can be calculated as the difference in formation energy of the two defects occupying neighboring sites in the lattice and the sum of the formation energies of the individual defects in the dilute limit as[5,11]

$$\Delta E^{\mathrm{int}} = \Delta E^{f}_{\mathrm{pair}} - \sum \Delta E^{f}_{\mathrm{isolated\ defects}}. \quad (6)$$

B. Environmental conditions

In order to calculate defect formation energies using Eqs. (1)–(5) we need to define the chemical potentials of the atoms being removed from, or added to, the system. These will in general depend on the processing conditions of the material. In this work, we assume that an atmosphere containing $\mathrm{O}_2(g)$ is present in all cases. At $T=0$ we may therefore define μ_{O} as half the total energy of an oxygen molecule—i.e.,

$$\mu_{\mathrm{O}} = \frac{1}{2}E^{\mathrm{tot}}[\mathrm{O}_2]. \quad (7)$$

Here $E^{\mathrm{tot}}[\mathrm{O}_2]$ is the total energy of an isolated oxygen dimer calculated using a sufficiently large supercell. We must also take into account that BaZrO_3 may exist within a range of chemical potentials for barium and zirconium. Two different limits will be considered[27]: In the Ba-rich limit, the system is in equilibrium with BaO(s). Then $\mu_{\mathrm{Ba}}=\mu_{\mathrm{Ba}}^{\mathrm{BaO}}\equiv E^{\mathrm{tot}}[\mathrm{BaO}]-\mu_{\mathrm{O}}$. To prevent precipitation of barium oxide, it is required that the chemical potential of barium be lower than this value—i.e.,

$$\mu_{\mathrm{Ba}} < \mu_{\mathrm{Ba}}^{\mathrm{BaO}}. \quad (8)$$

In the other extreme, the Zr-rich limit, the system is in equilibrium with $\mathrm{ZrO}_2(s)$. Then $\mu_{\mathrm{Zr}}=\mu_{\mathrm{Zr}}^{\mathrm{ZrO}_2}\equiv E^{\mathrm{tot}}[\mathrm{ZrO}_2]-2\mu_{\mathrm{O}}$ and $\mu_{\mathrm{Ba}}=E^{\mathrm{tot}}[\mathrm{BaZrO}_3]-\mu_{\mathrm{Zr}}^{\mathrm{ZrO}_2}-3\mu_{\mathrm{O}}$. Using the expression for the heat of formation for BaZrO_3 from the binary oxides [cf. Eq. (20)] the latter condition can be rewritten as $\mu_{\mathrm{Ba}}=\mu_{\mathrm{Ba}}^{\mathrm{BaO}}+\Delta E^{f}_{\mathrm{BaZrO}_3}$, where $\Delta E^{f}_{\mathrm{BaZrO}_3}$ is negative. The allowed range for μ_{Ba} is therefore

$$\mu_{\mathrm{Ba}}^{\mathrm{BaO}} + \Delta E^{f}_{\mathrm{BaZrO}_3} < \mu_{\mathrm{Ba}} < \mu_{\mathrm{Ba}}^{\mathrm{BaO}}. \quad (9)$$

For any value of the chemical potential for Ba within this range, the chemical potential for Zr must assume the value

$$\mu_{\mathrm{Zr}} = \mu_{\mathrm{Zr}}^{\mathrm{ZrO}_2} + \Delta E^{f}_{\mathrm{BaZrO}_3} + \mu_{\mathrm{Ba}}^{\mathrm{BaO}} - \mu_{\mathrm{Ba}}. \quad (10)$$

Finally, the atomic chemical potential of a dopant M can, in principle, be determined from the total energy of the corresponding binary oxide $M_2\mathrm{O}_3$.

In a semiconductor, the electronic chemical potential μ_{e} can assume values ranging from the energy of the valence band maximum, ϵ_{VBM}, to the energy of the conduction band minimum, ϵ_{CBM}. These limiting values of μ_{e} can in practical supercell calculations be obtained as the ground-state total-energy differences $\epsilon_{\mathrm{VBM}}=E^{\mathrm{tot}}[0]-E^{\mathrm{tot}}[+1]$ and $\epsilon_{\mathrm{CBM}}=E^{\mathrm{tot}}[-1]-E^{\mathrm{tot}}[0]$, where $E^{\mathrm{tot}}[q]$ denotes the total energy of a perfect lattice supercell where q electrons have been removed.[8,17]

C. Finite temperatures and pressures

The formation energies calculated using Eqs. (1)–(5) are strictly valid only at $T=0$, and they also exclude zero-point motion effects. In order to compare with experiments conducted at finite temperatures and pressures, the Gibb's free energy $G(p,T)$ has to be considered. At equilibrium and in the dilute limit, the concentration c of a particular defect is given by

$$c(p,T) = e^{-\Delta G^{f}(p,T)/k_{\mathrm{B}}T}, \quad (11)$$

where k_{B} is Boltzmann's constant,

$$\Delta G^{f}(p,T) = \Delta H^{f}(p,T) - T\Delta S^{f}(p,T), \quad (12)$$

and ΔH^{f} and ΔS^{f} are the change in enthalpy and entropy, respectively, associated with the formation of the defect.

For solids, in the harmonic approximation, the Gibbs free energy can be written as

$$G(p,T) = E^{\mathrm{tot}} + F^{\mathrm{vib}}(T), \tag{13}$$

where E^{tot} is the total electronic energy of the solid and $F^{\mathrm{vib}}(T)$ is the vibrational part. The latter is given by

$$F^{\mathrm{vib}}(T) = \sum_{s=1}^{3N} \left\{ \frac{\hbar\omega_s}{2} + k_B T \ln[1 - \exp(-\hbar\omega_s/k_B T)] \right\}, \tag{14}$$

where s runs over the $3N$ normal mode branches of frequency ω_s in a lattice of N atoms. When a defect is introduced, the associated change in vibrational free energy will in general have two distinct contributions: First, if an atom is removed (vacancy formation) or inserted (interstitial formation), the defective lattice will have a different number of vibrational modes compared with the perfect crystal. Second, the frequencies of the remaining modes may change in the presence of the defect. At high temperatures, this mainly contributes a change in entropy of the system.

Since we will consider a crystal in equilibrium with an oxygen atmosphere, atoms may be exchanged between the solid and gas phases when defects are formed. Assuming ideal gas behavior, the free energy per molecule O_2(g) is[28]

$$g_{O_2}(p,T) = h^0_{O_2}(T) - Ts^0_{O_2}(T) + k_B T \ln \frac{p}{p^0}, \tag{15}$$

where $h^0_{O_2}(T)$ and $s^0_{O_2}(T)$ are the enthalpy and absolute entropy, respectively, per molecule $O_2(g)$ at the reference partial pressure p^0. Since the electronic total energy obtained from DFT calculations corresponds to zero temperature, we set the reference enthalpy equal to the zero-point vibrational energy of an oxygen dimer—i.e., $h^0_{O_2}(T=0) = \hbar\omega_{O_2}/2$.

We will explicitly consider the formation of an oxygen vacancy by removing an oxygen from its lattice site and placing it in an oxygen dimer in the surrounding atmosphere. Then

$$\Delta G^{\mathrm{gas}}_{V_O}(p,T) = \frac{1}{2} g_{O_2}(p,T). \tag{16}$$

This decrease of the free energy of formation is partly compensated by an increase due to the reduction of the vibrational degrees of freedom of the crystal. For simplicity, we apply an Einstein model where it is assumed that all oxygen atoms in the perfect lattice have the same vibrational frequencies $\{\omega_{O,s}\}_{s=1}^3$ and that only the eight nearest neighbors are affected when a vacancy is introduced so that their vibrational frequencies change to $\{\omega'_{O,s}\}_{s=1}^3$. Using Eq. (14), the free energy of the three lattice modes that are missing in the defective crystal is

$$\Delta\widetilde{G}^{\mathrm{vib}}_{V_O}(T) = -\sum_{s=1}^{3} \left\{ \frac{\hbar\omega_{O,s}}{2} + k_B T \ln[1 - \exp(-\hbar\omega_{O,s}/k_B T)] \right\}, \tag{17}$$

and the change in vibrational free energy of the neighboring oxygens gives a contribution

$$\Delta G^{\mathrm{vib}}_{V_O}(T) = 8\sum_{s=1}^{3} \left\{ \frac{\hbar(\omega'_{O,s} - \omega_{O,s})}{2} + k_B T \ln\left[\frac{1 - \exp(-\hbar\omega'_{O,s}/k_B T)}{1 - \exp(-\hbar\omega_{O,s}/k_B T)} \right] \right\}. \tag{18}$$

Therefore, the oxygen vacancy free energy of formation can be written as

$$\Delta G^f_{V_O}(p,T) = \Delta E^f_{V_O} + \Delta\widetilde{G}^{\mathrm{vib}}_{V_O}(T) + \Delta G^{\mathrm{vib}}_{V_O}(T) + \Delta G^{\mathrm{gas}}_{V_O}(p,T), \tag{19}$$

where $\Delta E^f_{V_O}$ is the change in electronic total energy as given by Eq. (1), $\Delta\widetilde{G}^{\mathrm{vib}}_{V_O}(T)$ and $\Delta G^{\mathrm{vib}}_{V_O}(T)$ are the vibrational contributions defined by Eqs. (17) and (18), respectively, and $\Delta G^{\mathrm{gas}}_{V_O}(p,T)$ is the gas-phase contribution given by Eq. (16).

III. COMPUTATIONAL DETAILS

To investigate defect formation in $BaZrO_3$ we use DFT, which is the most widely used approach for electronic structure calculations of extended systems.[30] The success of this method is due to the availability of practical approximations for the crucial quantity represented by the exchange-correlation functional. In the present work, we employ a generalized gradient approximation (GGA) due to Perdew and Wang.[31] Such gradient-corrected functionals have been found to offer an adequate description of defect formation energies in perovskite-structured oxides when compared to a variety of other *ab initio* techniques.[9] The present calculations are performed using the plane-wave psuedopotential method as implemented in the Vienna *ab initio* simulation package (VASP).[32,33] The electron-ion interaction is described by the projector augmented-wave (PAW) method.[34] A plane-wave basis set with a cutoff energy of 400 eV was used in all calculations. Brillouin zone sampling was performed using a $6\times6\times6$ k-point grid for the five-atom primitive cell. Point defects were modeled using periodically repeated supercells consisting of either $2\times2\times2$ primitive cells (40 atoms) or $3\times3\times3$ primitive cells (135 atoms) with the number of k points reduced accordingly. This corresponds to a defect concentration of $c=1/8$ and $c=1/27$, respectively. In the simulations of charged defects, electrons were removed from or added to the supercell containing the defect. To avoid divergence of the Coulomb energy of the infinite crystal, the resulting electronic chargewas neutralized by the standard means of including a uniform "jellium" background charge in the cell.[29] Structural optimizations were performed at constant volume and under the condition that all residual forces should be smaller than 0.05 eV/Å. Vibrational frequencies were calculated within the harmonic approximation by evaluating and diagonalizing a dynamical matrix. Except for the O_2 molecule, spin polarization was generally not taken into account in the present study. However, although the electronic ground state of pure $BaZrO_3$ (Sec. IV A) is nonmagnetic, this cannot be assumed *a priori* for the investigated point defects in this material.[9] Therefore, we have also performed spin-polarized test calculations to check the accu-

TABLE I. Calculated equilibrium lattice parameter a_0 and corresponding heat of formation per formula unit E_0^{tot} compared with experimental data for the oxides $BaZrO_3$, BaO, and ZrO_2.

	a_0 (Å)		E_0^{tot} (eV/f.u.)	
Oxide	Theory	Expt.	Theory	Expt.
$BaZrO_3$	4.25	4.19[a]	−16.73	−18.102±0.004[b]
BaO	5.61	5.52[a]	−5.17	−5.663±0.022[c]
ZrO_2	5.15	5.26[a]	−10.25	−11.309±0.018[c]

[a]Reference 46.
[b]$T=0$ K (extrapolated), Ref. 47.
[c]$T=0$ K, Ref. 41.

racy of our results for vacancies (Sec. IV B) and dopant atoms (Sec. IV C).

IV. RESULTS AND DISCUSSION

A. Pure compounds

We first investigate the properties of pure $BaZrO_3$ (cubic perovskite lattice, space group $Pm\bar{3}m$). The equilibrium structure was determined by calculating the total energy for several different lattice parameters and fitting the data to Murnaghan's equation of state. The results are given in Table I. The equilibrium lattice parameter $a_0=4.25$ Å is close to the experimental result. The corresponding total energy, expressed as the heat of formation from the elements in their standard states (Ba: bcc, Zr: hcp, and O: dimer) is, however, slightly smaller than the experimental value. In order to determine the limits of the chemical potentials μ_{Ba} and μ_{Zr}, we also performed similar calculations for BaO (NaCl structure, space group $Fm\bar{3}m$) and ZrO_2 (fluorite structure, space group $Fm\bar{3}m$) in Table I. For all three investigated oxides, it is found that the calculated lattice parameters are within 2% of the experimental results, but that our choice of parametrization for the exchange-correlation functional tends to underestimate the binding energies (the GGA "underbinds" these systems). The difference is, however, less than 10%. A similar underbinding of several oxides by the GGA has also beenreported by Moriwake *et al.* in their study of doped lanthanum chromite.[16] We note, however, that our calculated heat of formation of $BaZrO_3$ from BaO and ZrO_2, defined as

$$\Delta E^{f}_{BaZrO_3} = E^{tot}[BaZrO_3] - E^{tot}[BaO] - E^{tot}[ZrO_2], \tag{20}$$

is −1.31 eV, in good agreement with the experimental value −1.33 eV.[35]

To check for structural instabilities of the ideal cubic perovskite structure, we have also calculated the Γ-point phonon frequencies of $BaZrO_3$. In addition to three zero-frequency acoustic modes, there are four three fold-degenerated optical modes. These are given in Table II. Generally, the obtained frequencies are lower than the experimental results. This may in part be due to the fact that the calculations were performed using the theoretical equilibrium lattice parameter (4.25 Å), which is slightly larger than the experimental value

TABLE II. Calculated phonon frequencies ν at the Γ point compared with experimental data (only three modes are optically active) for the cubic phase of $BaZrO_3$.

	ν (cm^{-1})	
Mode	Theory	Expt.[a]
Zr-O stretch	483	505
O-Zr-O bend	190	210
Zr-O_3 torsion	182	—
Ba-ZrO_3	91	115

[a]Reference 48.

(4.19 Å). However, since no imaginary frequencies were obtained, the cubic phase investigated in the present study is stable.

On a microscopic scale, defect formation is associated with changes in the electronic structure of a material. In Fig. 1 the calculated site-projected electronic density of states for a perfect $BaZrO_3$ crystal is shown. The lower valence bands consist of a mixture of Ba(5*s*) and Zr(4*p*) states around −25 eV, O(2*s*) states around −15 eV, and Ba(5*p*) states around −10 eV. The upper valence band extends down to approximately −4 eV and is composed mainly of O(2*p*) states with a small contribution from Zr(4*d*) states. This suggests that a moderate covalent bonding contribution is present in the crystal. The lower conduction band is mainly a mixture of Ba(5*d*) and Zr(4*d*) states, with a small admixture from O(2*p*). Our calculated electronic structure is in good agreement with earlier theoretical results of King-Smith and Vanderbilt[36] using ultrasoft pseudopotentials and more recently by Terki *et al.*[37] using a full-potential all-electron approach. The calculated band gap is around 3 eV, which is

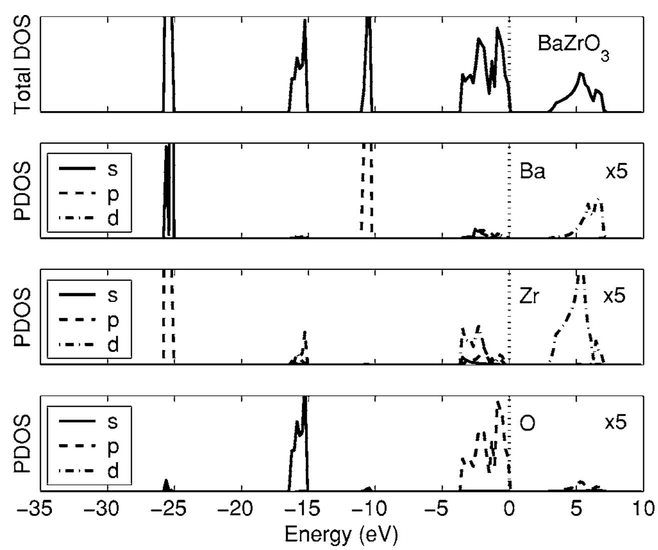

FIG. 1. Calculated total- and site-projected electronic density of states (DOS) for pure $BaZrO_3$. The energy of the highest occupied state is indicated by a dotted line. The valence band is composed mainly of O(2*p*) states, whereas the conduction band derives from Ba(5*d*) and Zr(4*d*) states. These are separated by a calculated band gap of around 3 eV.

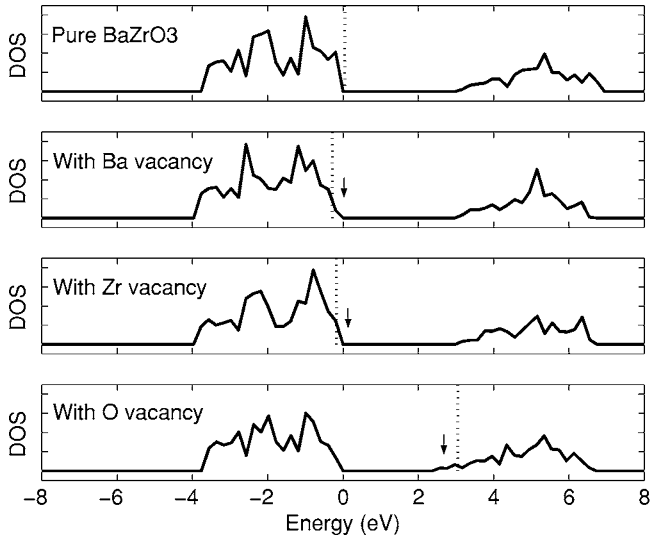

FIG. 2. Calculated electronic density of states around the band-gap region for $BaZrO_3$ with various point defects. The energy of the highest occupied state for each system is indicated by a dotted line. The removal of a Ba atom or a Zr atom introduces unoccupied states near the top of the valence band, whereas removal of an O atom introduces new levels in the band gap below the conduction band (as indicated by arrows).

significantly smaller than the experimental results 5.3 eV.[38] That the electronic band gaps of insulators and semiconductors come out grossly underestimated is a well-known artifact of the traditional DFT.[30] It is likely to affect the calculated formation energies of defects that introduce electrons in donor states with conduction band character.[27] Such results may be improved by a better treatment of the nonlocal exchange part of the total-energy functional (for instance, by using so-called exact exchange[39]) or, more heuristically, by a simple correction scheme where the conduction band is assumed to be rigidly shifted upward to match the experimental band gap. This will be discussed further in Secs. IV B and IV C.

B. Vacancies

We will next investigate the formation of vacancies in $BaZrO_3$. The electronic density of states for a crystal with different types of vacancies in the neutral charge state is shown in Fig. 2. In each graph, the highest occupied state is indicated by a dotted line. It is seen that the removal of a Ba atom or a Zr atom results in unoccupied states near the top of the valence band, indicating that cation vacancies behave as shallow acceptors in the material. By contrast, the removal of an O atom results in new occupied levels below the bottom of the conduction band, showing that oxygen vacancies instead behave as shallow donors. The observations are consistent with a simplified description of the $BaZrO_3$ crystal where each Ba donates two and each Zr four electrons to the filled oxygen p band. These electrons will be missing if a neutral metal atom is removed. If, on the other hand, a neutral oxygen is removed, there will be two electrons left behind in the metal d band.

TABLE III. Formation energy ΔE^f for vacancies in different charge states q in $BaZrO_3$ calculated using either a small $2\times2\times2$ supercell ($c=1/8$) or a larger $3\times3\times3$ supercell ($c=1/27$). For charged defects, the Fermi energy is taken as the energy of the top of the valence band ($\mu_e=\epsilon_{VBM}$).

Defect	Charge q	ΔE^f (eV) $c=1/8$		$c=1/27$	
V_O	0	6.57		6.55	
V_O	+2	1.21		1.21	
V_{Ba}	0	3.02[a]	1.71[b]	2.58[a]	1.27[b]
V_{Ba}	−2	2.13[a]	0.82[b]	2.25[a]	0.94[b]
V_{Zr}	0	4.48[a]	5.79[b]	4.03[a]	5.34[b]
V_{Zr}	−4	4.11[a]	5.42[b]	3.68[a]	4.99[b]

[a]Ba-rich conditions: $\mu_{Ba}=\mu_{Ba}^{BaO}$ and $\mu_{Zr}=\mu_{Zr}^{ZrO_2}+\Delta E^f[BaZrO_3]$.
[b]Zr-rich conditions: $\mu_{Ba}=\mu_{Ba}^{BaO}+\Delta E^f[BaZrO_3]$ and $\mu_{Zr}=\mu_{Zr}^{ZrO_2}$.

In Table III we report formation energies for Ba, Zr, and O vacancies in their neutral and fully ionized charge states calculated using Eqs. (1)–(3). For the chemical potentials, μ_O is uniquely defined by Eq. (7), while for μ_{Ba} and μ_{Zr} the two limiting values specified by Eqs. (9) and (10) have been considered: Barium vacancies have a lower formation energy under Zr-rich conditions (low μ_{Ba}) than under Ba-rich conditions (high μ_{Ba}), while zirconium vacancies are more easily formed under Ba-rich conditions (low μ_{Zr}) than under Zr-rich conditions (high μ_{Zr}). Moreover, supercells of two different sizes have been employed in order to investigate the concentration dependence of the formation energies. From the results given in Table III it is seen that the formation energy of oxygen vacancies is converged already with the smaller supercell ($c=1/8$), but to obtain the formation energy of cation vacancies in the dilute limit appears to require the use of the larger supercell ($c=1/27$).

For vacancies carrying a charge, the formation energy will also depend on the actual position of the Fermi level in the material. This is shown in Fig. 3 for $c=1/27$. As a result, oxygen vacancies in the +2 charge state are more easily formed than neutral oxygen vacancies in a p-type material where μ_e is close to the top of the valence band. Similarly, the formation energies of barium vacancies in the −2 charge state and zirconium vacancies in the −4 charge state are lower than the formation energies of the corresponding neutral vacancies in an n-type material where μ_e is close to the bottom of the conduction band.

Spin-polarized test calculations using different supercells were found to lower the formation energy of a neutral Zr vacancy by 0.30 eV ($c=1/8$) and 0.02 eV ($c=1/27$). For charged Zr vacancies and for Ba and O vacancies, the formation energies only changed by a few meV. This is consistent with the results of Ricci *et al.*[9] who investigated the formation of neutral oxygen vacancies in $SrTiO_3$ and paid particular attention to the possible existence of magnetic ground states and to spin localization phenomena. By carefully comparing the results of several different computational approaches (cluster and supercell calculations, using Hartree-Fock as well as and spin-polarized DFT with various ap-

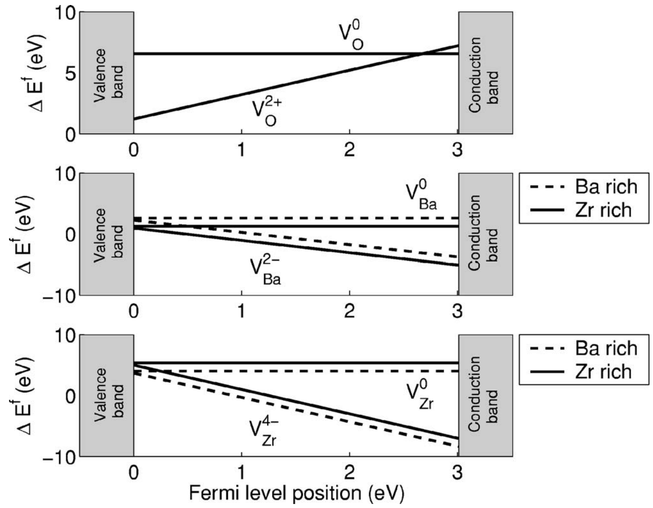

FIG. 3. Formation energies of vacancies in different charge states as a function of the Fermi-level position within the theoretical band gap of $BaZrO_3$ calculated using a supercell corresponding to a low defect concentration ($c=1/27$). For the cation vacancies, results are shown for the two limiting thermodynamical conditions of the Ba and Zr atomic chemical potentials: the Ba-rich and Zr-rich limits, respectively.

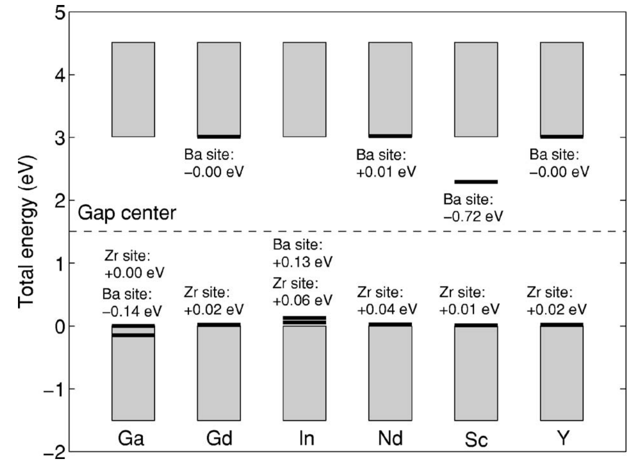

FIG. 4. Acceptor and donor levels corresponding to various dopant atoms incorporated on either Ba or Zr sites in $BaZrO_3$ calculated for a low defect concentration ($c=1/27$). Energies of defect levels below the gap center are given relative to the valence band maximum ϵ_{VBM}, whereas energies of the levels above the gap center are given relative to the conduction band minimum ϵ_{CBM}.

proximations for the exchange-correlation functional) it was found that the electronic ground state is indeed a nonmagnetic, closed-shell singlet state. However, since oxygen vacancies act as shallow donors in this material (cf. Fig. 2), we note that the position of the induced defect level may shift upward if the band gap error is corrected. This would increase the formation energy of a neutral oxygen vacancy (where the defect level is occupied by two electrons) but leave the formation energy of an oxygen vacancy in the +2 charge state (where the defect level is empty) unaffected. Nevertheless, our results appear to be in good agreement with previous studies: Ricci *et al.*[9] reported a formation energy of 6.8 eV with respect to $1/2 O_2$ for neutral oxygen vacancies in $SrTiO_3$, which is very similar to the 6.55 eV obtained in the present study (cf. Table III). Tanaka *et al.*[8] have calculated oxygen vacancy formation energies for several oxides with different crystal structure and found values in the range 1.5–7.1 eV (neutral charge state) and 0.3–2.4 eV (+2 charge state, $\mu_e=\epsilon_{VBM}$) for the normal phases under oxygen-rich conditions. We note that our results for $BaZrO_3$ also fall within these limits.

C. Dopant atoms

We will next consider the incorporation of Ga, Gd, In, Nd, Sc, and Y dopants on barium or zirconium sites in the lattice. Without specifying the actual value of the atomic chemical potentials μ_M, several general observations can be made about the behavior of these impurities in $BaZrO_3$.

First, it is possible to determine the position of the defect levels introduced in the band gap upon doping. These levels can be calculated as total-energy differences using Eq. (4) and (5) evaluated for different charge states of a particular dopant on a given site. A trivalent dopant M replacing a tetravalent Zr atom in the lattice can be expected to behave like an electronic acceptor: The Fermi-level position for which M_{Zr}^0 and M_{Zr}^- have the same solution energy defines the $0/-$ transition level for that dopant—i.e., the acceptor level ϵ_a. These results are shown in Fig. 4. For all the investigated elements, ϵ_a is close to (less than 0.06 eV above) ϵ_{VBM}. Allowing for spin-polarization only changes the solution energies by a few meV and thus does not affect any of the acceptor levels significantly. From inspection of the electronic structure, it is also seen that the presence of a dopant atom on a zirconium site introduces empty states with valence band character. Therefore, although the calculated ϵ_a admittedly correspond to very small energy differences, these results should not be very sensitive to the band gap error of the DFT. For a dopant replacing a divalent Ba atom in the lattice, the behavior is quite different: The donor level ϵ_d (i.e., the $+/0$ transition level) can be defined as the Fermi-level position where M_{Ba}^+ and M_{Ba}^0 have equal energies of solution. As shown in Fig. 4, the calculated ϵ_d is close to the bottom of the conduction band for the large dopants Gd, Nd, and Y, for Sc it is further down in the gap, and for Ga and In it is even close to the top of the valence band. Spin polarization was found to lower the solution energy of a neutral Sc dopant on a barium site by 0.11 eV (so that the corresponding donor level moves slightly closer to the gap center) but otherwise did not affect any of the results. Furthermore, if a band gap correction is applied, the positions of the shallow donor levels introduced by Gd, Nd, and Y can be expected to shift upward together with the conduction band so that the distance from ϵ_{CBM} remains unaffected.

Second, we may address the problem of site occupation—i.e., whether a particular dopant should prefer to substitute for Ba or Zr. From Eqs. (4) and (5) it is seen that μ_M cancels if one takes the difference of these solution energies, but the results will depend on μ_{Ba} and μ_{Zr}. The energy to incorporate a dopant on a Ba (Zr) site is lower under Zr (Ba) rich conditions than under Ba (Zr) rich conditions. This is similar

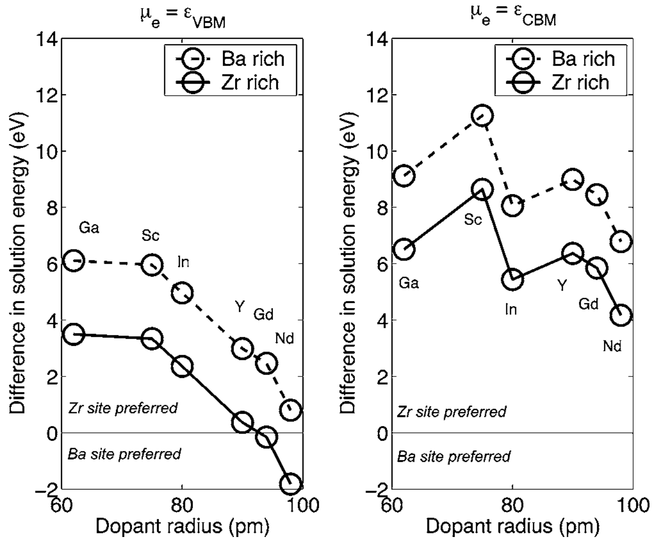

FIG. 5. Difference in solution energy for various dopants on Ba or Zr sites in $BaZrO_3$ calculated for a low defect concentration ($c=1/27$). Only the most stable charge state of each dopant on either site is considered. Results are shown for the two limiting values of the Fermi-level position within the theoretical band gap: $\mu_e=\epsilon_{VBM}$ and $\mu_e=\epsilon_{CBM}$.

to cation vacancy formation, since in both cases barium or zirconium is removed from the system. Site occupancy is also affected by the position of the Fermi level in the material, since this determines which charge state has the lowest energy for a dopant on a given site. For $\mu_e=\epsilon_{VBM}$, all acceptor levels and most donor levels (except that introduced by Ga) are empty (cf. Fig. 4). This means that dopants are present as M^0_{Zr} on Zr sites, but as M^+_{Ba} on Ba sites (except for M=Ga which is neutral). As μ_e increases through the band gap, more defect levels start to fill. For $\mu_e=\epsilon_{CBM}$, all acceptor levels and most donor levels (except that introduced by Nd) are occupied (cf. Fig. 4). This means that dopants are present as M^-_{Zr} on Zr sites but as M^0_{Ba}on Ba sites (except for M=Nd which is ionized). The difference in solution energy for the preferred charge state on Ba and on Zr sites is shown in Fig. 5 as a function of the ionic radius[40] of the dopant for the limiting environmental conditions, neglecting the temperature and pressure dependence on the allowed range for μ_{Ba} and μ_{Zr}. It is seen that in n-type $BaZrO_3$ ($\mu_e\approx\epsilon_{CBM}$) all the investigated dopants have the lowest solution energy on Zr sites. The doping then introduces acceptor levels (cf. Fig. 4) that lower the position of the Fermi level. Also in a predominantly p-type material ($\mu_e\approx\epsilon_{VBM}$) dopants with small ionic radii will prefer to substitute for Zr regardless of the environmental conditions. However, dopants with large ionic radii (such as Gd and Nd) will then instead have a lower solution energy when substituting for Ba if μ_{Zr} is high. This would increase the Fermi level until equilibrium is established with a fraction of the dopants occupying the Ba sites. We note that these general observations hold irregardless of the precise positions of the calculated defect levels (cf. Fig. 4).

That the solution of trivalent dopants in perovskite oxides is mainly driven by size effects has previously been shown

TABLE IV. Calculated interaction energies ΔE^{int} between dopant-dopant and dopant-oxygen vacancy pairs in $BaZrO_3$. A positive sign indicates a repulsive interaction, whereas a negative sign means that the defects tend to attract each other.

Dopant	ΔE^{int} (eV)	
M	$M^-_{Zr}\cdots M^-_{Zr}$	$M^-_{Zr}\cdots V^{2+}_O$
Ga	0.03	−0.68
Gd	0.35	−0.55
In	0.19	−0.62
Nd	0.64	−0.89
Sc	0.02	−0.37
Y	0.26	−0.45

from atomistic modeling using interatomic potentials.[4,5] Haile *et al.*[20] have discussed the possible influence of nonstoichiometry in doped ABO_3-type alkaline-earth cerates and zirconates and suggested that a divalent ion deficiency might drive the dopant incorporation onto the A site instead of the intended B site. This has been shown in a recent computational study of doped $BaCeO_3$ by Wu *et al.*[7] and is also in good agreement with our findings for $BaZrO_3$ in the present work.

D. Defect interactions

We will finally present data for and discuss the consequences of dopant-dopant and dopant-oxygen vacancy interactions in $BaZrO_3$. In Table IV we report the interaction energies for various defect pairs calculated using Eq. (6) and a $3\times3\times3$ supercell.

The dopant-dopant interactions were obtained as the difference in solution energy of a pair of dopants occupying neighboring Zr sites (total effective charge $q=-2$), and twice the solution energy of an isolated dopant on a Zr site ($q=-1$) from Eq. (5). As shown in the first column of Table IV, the interaction energies ΔE^{int} thus obtained are positive, which means that the dopants tend to repel each other. The strength of this repulsion is however strongly correlated with the size of the substitutional ion—ranging from weak (<0.05 eV) for dopants with approximately the same radius as Zr^{4+} to strong (0.65 eV) for the largest investigated dopant. This will have implications for the distribution of the dopant atoms in the lattice: For large impurities, the repulsion effectively obstructs dopants from occupying neighboring sites, whereas for small impurities the repulsion is much more moderate and the dopants may be more randomly distributed.

The dopant–oxygen-vacancy interactions were similarly obtained as the difference in formation energy of a dopant on a Zr site with a neighboring oxygen vacancy (total effective charge $q=+1$) and the sum of the formation energies of an isolated dopant on a Zr site ($q=-1$) from Eq. (5) and an isolated oxygen vacancy ($q=+2$) from Eq. (1). As shown in the second column of Table IV, the interaction energies ΔE^{int} thus obtained are negative, which means that dopant atoms and oxygen vacancies tend to attract each other and a "trapping" of oxygen vacancies near the dopant sites in the material might occur. This would affect the activation energy for oxide ion migration (which take place via a vacancy-mediated mechanism),[4] as well as the hydration enthalpy (where water molecules are dissociatively incorporated into oxygen vacancies).[2]

To check our results, we have also compared the interaction energies calculated using Eq. (6) with the difference in total energy of a large supercell when the defects are nearest neighbors or as far separated as possible (taking periodicity into account) and obtained very similar results. Moreover, our dopant-oxygen vacancy interaction energies are comparable in magnitude to those found in previous studies: For CeO_2, the DFT results of Skorodumova *et al.*[14] give a binding energy of an oxygen vacancy and two Ce(3+) atoms (which effectively act as dopants) equal to −1.43 eV. Based on atomistic modeling using interatomic potentials, Mather and Islam[6] recently reported binding energies ranging from −0.75 to −0.95 eV for a pair cluster and from −0.95 to −1.25 eV for a trimer cluster in acceptor-doped $SrCeO_3$. Finally, we note that a similar attractive interaction has also been found for pairs consisting of a dopant atom and a protonic defect.[11]

E. Defect structure at finite (p,T)

From the results given in Sec. IV C it is clear that most of the investigated dopants will predominantly incorporate on Zr sites in $BaZrO_3$ at $T=0$. When fully ionized, these dopants will act as negatively charged defects in the material. The dominating charge-compensating defects are then expected to be either electronic holes or oxygen vacancies. However, oxygen vacancies are not expected to appear since $\Delta E^f_{V_O} > 0$ for all Fermi-level positions as shown in Sec. IV B. For instance, the formation energy of an oxygen vacancy in the +2 charge state is equal to +1.2 eV in *p*-type $BaZrO_3$ where $\mu_e \approx \epsilon_{VBM}$ (cf. Table III) and even higher for other values of μ_e (cf. Fig. 3). If a complete dopant-oxygen vacancy association is assumed, $\Delta E^f_{V_O}$ might be reduced by 0.4–0.9 eV compared to the case of noninteracting defects (cf. Table IV), but for none of the investigated dopants is the magnitude of this interaction sufficiently large to make oxygen vacancies form in any appreciable concentrations at $T=0$. This is analogous to the situation for alkaline-earth-doped lanthanum chromites, where Moriwake *et al.*[16] demonstrated that the solution energies for ionized and charge-compensated dopants are much higher than for neutral dopants.

It is now important to take into account that our system is in equilibrium with a gas phase at finite oxygen pressure p and temperature T. The oxygen vacancy formation is then governed by the change in Gibb's free energy $\Delta G^f_{V_O}(p,T)$ as given by Eq. (19). The frequencies needed for the vibrational contributions were determined by performing harmonic analysis on individual atoms in a $2\times2\times2$ supercell with and without an oxygen vacancy in the +2 charge state. We obtained $\hbar\omega_O=69$, 31, and 31 meV for an oxygen atom in the perfect lattice and $\hbar\omega'_O=66$, 34, and 29 meV for an oxygen atom close to a vacancy. For the gas-phase contribution, the temperature dependence for $h^0_{O_2}$ and $s^0_{O_2}$ was taken from thermodynamical tables.[41] The resulting free energy of formation per formed oxygen vacancy is shown in Fig. 6 as a function of T at constant pressure. At low temperatures, $\Delta G^f > 0$ due to the positive contribution from the change in electronic total energy. However, at high temperatures, the remaining terms in Eq. (19) become sufficiently negative to bring $\Delta G^f < 0$. The dominating contribution to the free energy of formation then comes from the entropy increase associated with the release of gas molecules to the atmosphere. The change in vibrational free energy of the lattice is smaller and is dominated by the loss of the three lattice modes. For instance, $T=1500$ K (which is a realistic sintering temperature) and $p=0.2$ atm gives $\Delta G^{vib}+\Delta\widetilde{G}^{vib}=0.4$ eV, $\Delta G^{gas}=-1.8$ eV, and thus $\Delta G^f=-0.2$ eV. In Fig. 7 it is shown that ΔG^f can also be reduced by a lowering of the oxygen partial

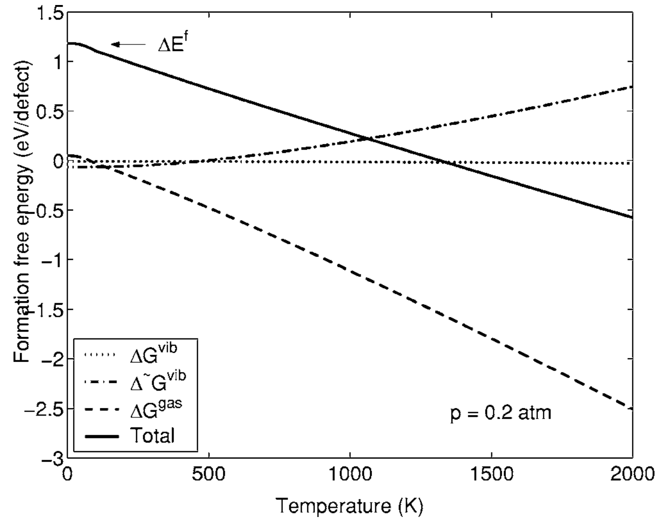

FIG. 6. The calculated electronic (ΔE^f), vibrational (ΔG^{vib} and $\Delta\widetilde{G}^{vib}$), and gas-phase ($\Delta G^{gas}$) contributions to the free energy of formation for an oxygen vacancy in $BaZrO_3$ as a function of temperature at a constant oxygen partial pressure $p=0.2$ atm.

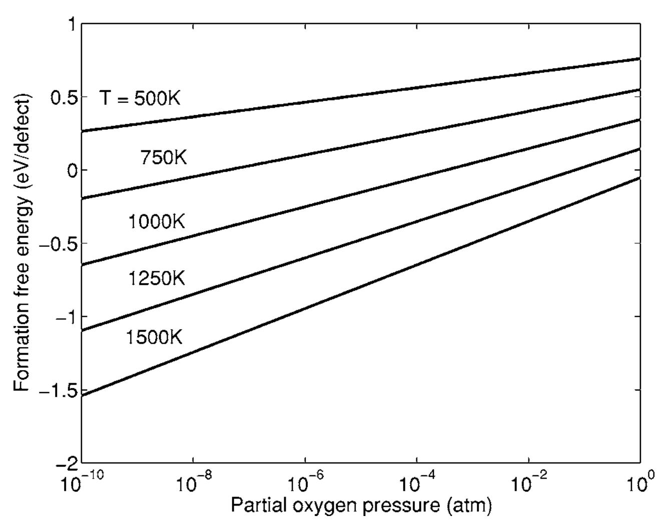

FIG. 7. The calculated free energy of formation for an oxygen vacancy in $BaZrO_3$ as a function of the partial oxygen pressure at different constant temperatures T in the range 500–1500 K.

pressure at constant temperature. Our observation that the free energy of oxygen vacancy formation is dominated by ΔG^{gas} motivates the approach used by Kuwabara and Tanaka[17] in their theoretical investigation of the defect structure of $LaGaO_3$: By considering only the electronic total-energy and gas-phase contributions, it was shown that doping the oxide with lower valence elements results in electronic hole formation at low temperatures, but oxygen vacancy formation at high temperatures.

From Eq. (11) it is seen that the equilibrium concentration of oxygen vacancies grows rapidly when the temperature is increased or the partial oxygen pressure lowered so that ΔG^f decreases. Eventually, oxygen vacancies become the dominating charge-compensating defects, and their concentration will then be fixed to approximately one-half of the effective dopant concentration. As discussed above, this is likely to occur under typical processing conditions of perovskite oxides. Upon subsequent cooling, oxygen from the atmosphere may start to incorporate on the vacant oxygen sites so that electronic holes ($h^{\cdot}$) are formed according to

$$\frac{1}{2}\mathrm{O}_2(g) + \mathrm{V}_{\mathrm{O}}^{\cdot\cdot} \rightleftarrows \mathrm{O}_{\mathrm{O}}^{\times} + 2h^{\cdot}. \qquad (21)$$

This is in good agreement with data from thermogravimetric analysis showing that $BaZrO_3$ samples gain weight during cooling in a dry atmosphere.[22,42] However, at low temperatures the rate of oxygen incorporation reaction (21) may become limited by slow surface kinetics and/or bulk diffusion rates. The vacancy concentration then becomes "frozen in" at a value that depends sensitively on the processing conditions prior to the quenching.[43] This is also consistent with the experimental observations that acceptor-doped zirconates are mixed oxide ion and *p*-type electrical conductors under dry conditions.[22–24,42,44]

V. CONCLUSIONS AND OUTLOOK

To summarize, we have combined density functional calculations and thermodynamic modeling to investigate defect formation in a perovskite oxide in equilibrium with an oxygen-containing atmosphere. We have presented results for anion and cation vacancies and for Ga, Gd, In, Nd, Sc, and Y dopants occupying either Ba or Zr sites in $BaZrO_3$. Formation energies have been evaluated for defects in different charge states and for different environmental conditions. We find that most of the investigated dopants preferably incorporate on Zr sites in the lattice, but that large dopants (such as Gd and Nd) may partly occupy Ba sites under Zr-rich conditions. The interaction between pairs of dopants was found to be repulsive and correlated with the ionic radius of the dopant, while the dopant-oxygen vacancy interaction was found attractive. Our results also show that oxygen vacancies are not thermodynamically stable at low temperatures, even for an acceptor-doped material. Rather, the vacancies are expected to appear as charge-compensating defects only at the high temperatures typically used during synthesis of perovskite oxides. $BaZrO_3$ cooled in air may therefore show mixed electron-hole or oxygen ion conductivity, depending on the thermal history of the sample.

In the presence of a humid atmosphere, also the formation of protonic defects in acceptor-doped perovskite oxides must be considered.[2,3,11] The thermodynamic stability and mobility of such defects will be investigated in a forthcoming study.[45]

ACKNOWLEDGMENTS

This work was supported by the National Graduate Schools in Scientific Computing and Material Science and by the Foundation for Strategic Research via the ATOMICS program, Sweden. Allocations of computer resources through the Swedish National Allocation Committee are gratefully acknowledged.

[1] H. Iwahara, in *Proton Conductors: Solids, Membranes and Gels—Materials and Devices*, edited by P. Colomban (Cambridge University Press, Cambridge, England, 1992), Chap. 8.
[2] K. D. Kreuer, Solid State Ionics **97**, 1 (1997).
[3] T. Norby and Y. Larring, Curr. Opin. Solid State Mater. Sci. **2**, 593 (1997).
[4] R. A. Davies, M. S. Islam, and J. D. Gale, Solid State Ionics **126**, 323 (1999).
[5] M. S. Islam, P. R. Slater, J. R. Tolchard, and T. Dinges, Dalton Trans. 3061 (2004).
[6] G. C. Mather and M. S. Islam, Chem. Mater. **17**, 1736 (2005).
[7] J. Wu, R. A. Davies, M. S. Islam, and S. M. Haile, Chem. Mater. **17**, 846 (2005).
[8] I. Tanaka, F. Oba, K. Tatsumi, M. Kunisu, M. Nakano, and H. Adachi, Mater. Trans. **43**, 1426 (2002).
[9] D. Ricci, G. Bano, G. Pacchioni, and F. Illas, Phys. Rev. B **68**, 224105 (2003).
[10] J. Carrasco, N. Lopez, and F. Illas, J. Chem. Phys. **122**, 224705 (2005).
[11] M. S. Islam, R. A. Davies, and J. D. Gale, Chem. Mater. **13**, 2049 (2001).
[12] H. Yukawa, K. Nakatsuka, and M. Morinaga, Solid State Ionics **116**, 89 (1999).
[13] M. Yoshino, K. Nakatsuka, H. Yukawa, and M. Morinaga, Solid State Ionics **127**, 109 (2000).
[14] N. V. Skorodumova, S. I. Simak, B. I. Lundqvist, I. A. Abrikosov, and B. Johansson, Phys. Rev. Lett. **89**, 166601 (2002).
[15] C. Stampfl, M. V. Ganduglia-Pirovano, K. Reuter, and M. Scheffler, Surf. Sci. **500**, 368 (2002).
[16] H. Moriwake, I. Tanaka, K. Tatsumi, Y. Koyama, H. Adachi, H. Yakabe, and I. Yasuda, Mater. Trans. **43**, 1456 (2002).
[17] A. Kuwabara and I. Tanaka, J. Phys. Chem. B **108**, 9168 (2004).
[18] K. D. Kreuer, Solid State Ionics **125**, 285 (1999).
[19] K. D. Kreuer, S. Adams, W. Münch, A. Fuchs, U. Klock, and J. Maier, Solid State Ionics **145**, 295 (2001).
[20] S. M. Haile, G. Staneff, and K. H. Ryu, J. Mater. Sci. **36**,

1149 (2001).
[21] R. C. T. Slade, S. D. Flint, and N. Singh, Solid State Ionics **82**, 135 (1995).
[22] H. G. Bohn and T. Schober, J. Am. Ceram. Soc. **83**, 768 (2000).
[23] W. Wang and A. V. Virkar, J. Power Sources **142**, 1 (2005).
[24] V. P. Gorelov, V. B. Balakireva, Y. N. Kleschev, and V. P. Brusentsov, Inorg. Mater. **37**, 535 (2001).
[25] D. B. Laks, C. G. Van de Walle, G. F. Neumark, P. E. Blöchl, and S. T. Pantelides, Phys. Rev. B **45**, 10965 (1992).
[26] C. G. Van de Walle, D. B. Laks, G. F. Neumark, and S. T. Pantelides, Phys. Rev. B **47**, 9425 (1993).
[27] A. F. Kohan, G. Ceder, D. Morgan, and C. G. Van de Walle, Phys. Rev. B **61**, 15019 (2000).
[28] K. Reuter and M. Scheffler, Phys. Rev. B **65**, 035406 (2001).
[29] J. Lento, J.-L. Mozos, and R. M. Nieminen, J. Phys.: Condens. Matter **14**, 2637 (2002).
[30] R. M. Martin, *Electronic Structure: Basic Theory and Practical Methods* (Cambridge University Press, Cambridge, England, 2004).
[31] J. P. Perdew and Y. Wang, Phys. Rev. B **45**, 13244 (1992).
[32] G. Kresse and J. Hafner, Phys. Rev. B **48**, 13115 (1993).
[33] G. Kresse and J. Furthmüller, Phys. Rev. B **54**, 11169 (1996).
[34] P. E. Blöchl, Phys. Rev. B **50**, 17953 (1994).
[35] K. T. Jacob and Y. Waseda, Metall. Mater. Trans. B **26**, 775 (1995).
[36] R. D. King-Smith and D. Vanderbilt, Phys. Rev. B **49**, 5828 (1994).
[37] R. Terki, H. Feraoun, G. Bertrand, and H. Aourag, Phys. Status Solidi B **242**, 1054 (2005).
[38] J. Robertson, J. Vac. Sci. Technol. B **18**, 1785 (2000).
[39] M. Städele, M. Moukara, J. A. Majewski, P. Vogl, and A. Görling, Phys. Rev. B **59**, 10031 (1999).
[40] R. D. Shannon, Acta Crystallogr., Sect. A: Cryst. Phys., Diffr., Theor. Gen. Crystallogr. **32**, 751 (1976).
[41] M. W. Chase, *JANAF Thermochemical Tables*, 3rd ed. (American Chemical Society and the American Institute of Physics, New York, 1986).
[42] A. Manthiram, J. F. Kuo, and J. B. Goodenough, Solid State Ionics **62**, 225 (1993).
[43] I. Denk, W. Münch, and J. Maier, J. Am. Ceram. Soc. **78**, 3265 (1995).
[44] J. A. Labrincha, J. R. Frade, and F. M. B. Marques, Solid State Ionics **61**, 71 (1993).
[45] M. E. Björketun, P. G. Sundell, and G. Wahnström (unpublished).
[46] W. Pies and A. Weiss, in *Landolt-Börnstein: Numerical Data and Functional Relationships in Science and Technology*, edited by K.-H. Hellweg and A. M. Hellwege, New Series, Group III, Vols. 7b1 (Springer, Berlin, 1975) and 7e (Springer, Berlin, 1975).
[47] T. Matsui, Thermochim. Acta **253**, 155 (1995).
[48] C. H. Perry, D. J. McCarthy, and G. Rupprecht, Phys. Rev. **138**, A1537 (1965).